FERMILAB-PUB-76-106-E

~~Submitted~~ accepted to Nuclear Physics B, September, 1976.

PUB-76-106-E E-0002

E-2B

Semi-Inclusive π^- Cross Sections in pp Interactions up to 300 GeV/c

B. Y. Oh, M. Pratap, G. Sionakides, G. A. Smith and J. Whitmore
Department of Physics
Michigan State University*, East Lansing, Michigan 48824, U.S.A.

R. J. Miller, J. J. Phelan and P. F. Schultz
Argonne National Laboratory†
Argonne, Illinois 60439, U.S.A.

L. Voyvodic and R. J. Walker
Fermi National Accelerator Laboratory†
Batavia, Illinois 60510, U.S.A.

E. W. Anderson, H. B. Crawley, A. Firestone
W. J. Kernan, F. Ogino‡ and D. L. Parker
Department of Physics and Ames Laboratory, ERDA
Iowa State University†, Ames, Iowa 50010, U.S.A.

D. G. Hill**, M. Kazuno, G. McClellan, H. L. Price,
B. Sechi-Zorn, G. A. Snow and F. Svrcek
Department of Physics
University of Maryland†, College Park, Maryland 20742, U.S.A.

ABSTRACT

Semi-inclusive π^- cross sections in 200 and 300 GeV/c pp interactions are presented and compared with lower energy data. In the target fragmentation region the data are compared to the hypothesis of semi-inclusive KNO scaling. The energy and charge multiplicity dependences of the semi-inclusive cross sections in the central region are studied and a simple parametrization of the semi-inclusive density function is described.

---

*Work supported by the U.S. National Science Foundation.

†Work supported by the U.S. Energy Research and Development Administration.

‡Present address: Department of Physics, Purdue University.
W. Lafayette, Indiana 47907, U.S.A.

**Present address: Pfizer Medical Systems, Columbia, Maryland 21045, U.S.A.

1. Introduction

Single particle spectra from the semi-inclusive reaction

$$pp \rightarrow \pi^- + (n-1) \text{ charged} + \text{anything} \qquad (1)$$

are reported in this paper using 200 and 300 GeV/c data obtained in the Fermilab 30-inch bubble chamber-wide gap spark chamber hybrid system[1]. These data form a natural extension of the inclusive spectra from the process[2,3]

$$pp \rightarrow \pi^- + \text{anything}, \qquad (2)$$

particularly since there is a significant dependence on the charged multiplicity in high energy hadronic interactions.

In Section 2 we discuss the data sample used in this analysis. We present in Section 3 the rapidity and transverse momentum distributions for different charged multiplicity reactions. In Section 4 we present a test of semi-inclusive Koba-Nielsen-Olesen (KNO) scaling[4] in the target fragmentation region where, to a first approximation, inclusive scaling is known to hold. In Section 5 we turn to the systematics of the central region and attempt to answer the following questions: What is the energy and charged multiplicity dependence of the semi-inclusive cross sections and is the inclusive cross section approaching asymptotic scaling with an $s^{-1/4}$ behavior?

2. Experimental Details

The results reported here come from a total of 21,887 events of 200 and 300 GeV/c pp interactions and are listed in Table 1 in terms of the negative particle multiplicity, n_-. After two measurement passes, 97% (50%) of the four-prong ($\geq$ twenty-prong) events were successfully measured, with the trend monotonically decreasing with increasing charged multiplicity.

The events from each charged multiplicity have been subsequently normalized to published topological cross sections[5]. In this analysis each negative particle has been called a π^- and the K^- contamination has been subtracted from the negative particle spectra by utilizing K^- production data at a center of mass energy $\sqrt{s}$ = 23 GeV.[6] Since no semi-inclusive K^- data have been published we have assumed that the K^- spectra are independent of n_-.

The resulting π^- momentum spectra were studied separately in the forward and backward hemispheres in terms of the rapidity and transverse momentum squared variables. The required symmetry between backward and forward hemispheres in pp interactions is an excellent indicator of the possible effects of experimental resolution on the results quoted in this paper. In this regard, it is observed that the cm rapidity (y_{cm}) spectrum is symmetric around zero for $y_{cm} \lesssim 3$ and the transverse momentum squared distributions in the two hemispheres agree with each other up to $\sim$0.6 $(GeV/c)^2$, but disagree significantly beyond $\sim$1 $(GeV/c)^2$, particularly for $y_{cm} \gtrsim 3$. Thus, in all the data except for Figure 7(d), where only the backward hemisphere is used, we have utilized tracks from both hemispheres. For this study no significant differences between data utilizing only the "bare" bubble chamber and those utilizing the bubble chamber and the downstream spark chambers were detected. Hence, in order to optimize statistics the "bare" bubble chamber data are reported in this study.

3. Single Particle Spectra

Inclusive particle spectra of reaction (2) have received considerable attention, largely stimulated by the concept of possible scaling in high energy interactions.[7] However, high energy data on the corresponding semi-inclusive reactions are somewhat sparse in the literature.[8] In this

section we present π^- spectra from reaction (1) in terms of the laboratory rapidity (y_{lab}) and transverse momentum (p_T) variables. For comparison with lower energies, we use pp data at 21, 24 and 28.5 GeV/c.[9]

We plot in Fig. 1(a) $d\sigma/dy_{lab}$ for reaction (2) at 28.5, 200 and 300 GeV/c. It is seen that scaling holds rather well in the region $y_{lab} < 1$. More detailed analyses[10] of the inclusive data in the fragmentation region have shown an $s^{-1/2}$ behavior in the approach to scaling, consistent with the Mueller-Regge theory.[7] The inclusive transverse momentum distributions, $d\sigma/dp_T^2$, shown in Fig. 1(b) are similar in shape but grow in magnitude with increasing s. However, in the region $y_{lab} < 1$ this cross section appears to be independent of energy for $p_T^2 \lesssim 0.2\ (\mathrm{GeV/c})^2$. For $p_T^2 \gtrsim 0.2\ (\mathrm{GeV/c})^2$ the cross section appears to increase between 28.5 GeV/c and 200 and 300 GeV/c.

The charged multiplicity dependence of the y_{lab} and p_T^2 spectra are presented in Figs. 2 and 3 respectively, in terms of the densities

$$F_n(y_{lab},s) = \frac{1}{\sigma_n}\frac{d\sigma_n}{dy_{lab}} \tag{3}$$

and

$$G_n(p_T^2,s) = \frac{1}{\sigma_n}\frac{d\sigma_n}{dp_T^2}\,. \tag{4}$$

Also shown in Figs. 2 and 3 are lower energy semi-inclusive data.[9] The dominant features of these data are: (a) the four prong ($n_-=1$) data show a broad minimum in the central region unlike any of the higher multiplicity spectra shown in Fig. 2. This feature is also absent in the lower energy data and is presumably due to diffractive processes which dominate the four prong events at higher energy; (b) for $n_- \geq 2$ the shape and width of $F_n(y_{lab})$ vary mildly with n_-. Except for the target and beam fragmentation regions, F_n can be fitted to a Gaussian form, with the width parameter decreasing

slowly with increasing n_-; and (c) no appreciable dependence on n_- is observed in the shape of $G_n(p_T^2)$. However, at the detailed level, the average transverse momentum is observed to increase with energy and, at a given energy, decreases with increasing n_-. We defer further discussion of these and other systematics in the central region to section 5 of this paper.

4. KNO Scaling

In 1971, Koba et al.[4] proposed that the π^- invariant cross section of reaction (1) depends on the charged multiplicity only through the variable $z \equiv n_-/\langle n_- \rangle$:

$$\frac{1}{\sigma_n} \frac{d\sigma_n}{dy dp_T^2} = h(y,p_T^2,z) \left[1 + O\left(\frac{1}{\ln s}\right)\right] , \tag{5}$$

for $s \to \infty$ and n sufficiently large ($n \gtrsim \langle n \rangle$), provided that scaling is valid in the inclusive reaction (2). Soon after the initial operation at Fermilab, Ma et al.[11] tested this prediction with preliminary data from an exploratory pp experiment at 205 GeV/c and found the general trend of the data in the fragmentation region to be in reasonable agreement with this prediction. In Fig. 1 we have shown that the scaling hypothesis for inclusive π^- production is rather well satisfied in the restricted region $y_{lab} < 1$. It is now of interest to investigate with high statistics whether the semi-inclusive KNO scaling as suggested by Ma et al. holds in this region.

To improve the statistical accuracy of the investigation we propose to test this scaling in y_{lab} and p_T^2 separately. Namely, we investigate the behavior of the functions

$$F_n(y_{lab},s) \xrightarrow[s \to \infty]{} f(y_{lab},z) \tag{6}$$

and $$G_n(p_T^2,s) \xrightarrow[s \to \infty]{} g(p_T^2,z). \tag{7}$$

A number of lower energy data with similar z values as the corresponding high energy data have been plotted in Fig. 2 for the full kinematic range of the rapidity variable. We see that for $y_{lab} < 1$ the lower and higher energy data generally agree.

In Figures 4 and 5 we study in more detail the F_n and G_n functions, the latter with a cut $y_{lab}' < 1$, for z values closely matched between lower and higher energies. In these figures, (a-h) refer to the data sets in increasing order of z values as listed in Table 2. The general behavior of these functions is such that in the region $y_{lab} < 1$, the lower energy data approximately agree with, but lie slightly above, the higher energy data.

As an alternative test of the scaling and in a way which is more sensitive to the variations in z, we show in Fig. 6 the function $F_n(y_{lab},s)$ versus z at fixed regions of y_{lab} for different energies. In the region $y_{lab} < 1$ the F_n function decreases with increasing energy for all z values, except possibly for very low z. On the other hand, in the region $1 < y_{lab} < 2$ and for $z < 2$ we note little variation with energy (for $z > 2$ the high energy data indicate a fall-off with z, which is consistent with the effect of phase space restrictions on high multiplicity events). Thus the data taken as a whole present a somewhat complicated picture of a possible semi-inclusive scaling with different approaches to scaling with energy for different regions of the kinematic variables studied.

5. Central Region

At high energy, the inclusive π^- invariant cross section is known to rise with increasing s in the central region. Whether it is approaching an

asymptotic limit (such as the $A - |B|s^{-1/4}$ form[12] as expected in the Mueller-Regge theory) or increasing indefinitely[13,14] is by no means established. Much less known is the energy dependence of the semi-inclusive cross sections in the central region and the nature of their individual contributions towards the inclusive cross section in this region. These are the questions on which we focus our attention in this section.

First we study the variation with n_- of $F_n(y_{cm}=0)$ and $G_n(p_T^2=0)$, as well as the width (defined as full-width at half-maximum) of F_n and the average values of p_T^2, $\langle p_T^2 \rangle$. As shown in Figs. 7(a) and (b), $F_n(0)$ and $G_n(0)$ are approximately linear with n_-. The width of the F_n function and p_T^2 (Figs. 7(c) and (d)*) both decrease slowly with n_-. Furthermore, for fixed n_-, $F_n(0)$ decreases with increasing s roughly as $\ln^{-1}(s/m_p^2)$, the inverse of the rapidity range. The energy dependence of $G_n(0)$ is less extreme than that of $F_n(0)$. We note that $G_n(0)$ as studied here is not just for the central region, but is integrated over all values of rapidity.

We find that the s and n_- dependence of $F_n(0)$ is fitted well by the form

$$F_n(0) = \frac{1}{\ln(E_a^2/m_p^2)} \left(-0.8 + 1.6n_- + 0.05n_-^2\right) , \qquad (8)$$

where $E_a \equiv \sqrt{s} - 2m_p$ is the available energy and n_- ranges between 1 and 9. The validity of this expression is established by comparison with the data in Fig. 9, where $F_n(0)$ is plotted versus $\ln^{-1}(E_a^2/m_p^2)$ for various n_-. Equation (8) is represented by the straight lines in Fig. 8.

---

*As indicated previously, only backward hemisphere tracks have been used to calculate $\langle p_T^2 \rangle$. An additional cut of $p_T^2 < 4\ (\mathrm{GeV}/c)^2$ has been imposed to remove a very few tracks with high values of p_T whose measurement is thought to be in error.

The inclusive cross section at $y_{cm} = 0$ can be calculated from Eq. (8) if we know the s-dependence of <n>, the average charged multiplicity, and if we assume KNO multiplicity scaling.[15] To be explicit, we take the energy dependence of <n> for pp interactions to be of the form[3]

$$\langle n \rangle = 2.45 + 0.32 \ln E_a + 0.53 \ln^2 E_a \tag{9}$$

and the KNO multiplicity function to be of the form[16]

$$\sigma_n = \frac{\sigma_{inel}}{\langle n \rangle} \Psi \left(\frac{n}{\langle n \rangle}\right) , \tag{10}$$

with $\Psi(\omega) = \exp(-3.04\omega) \cdot (3.79\omega + 33.7\omega^3 - 6.64\omega^5 + 0.332\omega^7)$

and $\sigma_{inel} = 33$ mb.

The inclusive cross section $d\sigma/dy_{cm}$ at $y_{cm} = 0$, as calculated from Eqs. (8-10), is plotted as the solid curve in Fig. 9 together with the available data[6,8]#. A similar calculation without the $0.05\, n_-^2$ term of Eq. (8) is shown as the dotted curve for the purpose of comparison. We remark that an s-dependent total inelastic cross section (rather than the constant value of 33 mb) would predict the inclusive cross section to rise with energy faster than that shown by the curves in Fig. 9. On the other hand, the energy dependence of <n> as given by Eq. (9) is not well established beyond $\sqrt{s} = 28$ GeV.

The rapidity distribution can be well approximated (except for the regions of target and beam fragmentation defined by $|y_{cm}| \gtrsim 2$) by the Gaussian form

$$F_n(y_{cm}) = n_- \cdot \frac{\exp(-y_{cm}^2/2\delta_n^2)}{\delta_n\sqrt{2\pi}} , \tag{11}$$

#For the data of Alper et al. (Ref. 6), the fits given in Table 3 of their paper were numerically integrated over p_T^2.

with $$\delta_n \equiv \frac{n_-}{F_n(0)\sqrt{2\pi}} = \frac{\ln(E_a^2/m_p^2)}{\sqrt{2\pi}(-0.8/n_- + 1.6 + 0.05n_-)} \tag{12}$$

This expression for the width describes the energy and n_- dependences of the semi-inclusive cross sections and, by summation of the different multiplicity distributions, the s-dependence of the inclusive π^- cross sections. The width of the inclusive rapidity distribution thus obtained is compared with the experimentally determined width as a solid curve in Fig. 10. It reproduces the experimental width reasonably well up to $p_{lab} \sim 400$ GeV/c. Also shown in Fig. 10 for comparison is the prediction of the hydrodynamic model[13],

$$\delta_{hyd} = \sqrt{\ln(\sqrt{s}/2m_p)} \ , \tag{13}$$

as a dotted curve. The agreement between the hydrodynamic model and the results of our parametrization is interesting, considering the different energy dependences in Eqs. (12) and (13). The trend of the data indicates that both calculations may possibly underestimate the experimental width at very high energy.

6. Conclusions

We have presented a study of the energy dependence of semi-inclusive π^- data from pp interactions. In the target fragmentation region the 200 and 300 GeV/c data, together with lower energy data, indicate a possible semi-inclusive KNO scaling with different approaches to scaling with energy for different regions of the kinematic variables studied.

In the central region we have described a relatively simple parametrization of the energy and charged particle multiplicity dependences of the

semi-inclusive density functions, and by summation of the different multiplicity distributions, the energy dependence of the inclusive π^- cross sections. The results of this parametrization suggest that the inclusive cross section in the central region increases faster than the $A - |B|\ s^{-1/4}$ form in the Fermilab-ISR energy region.

We thank the staff at Fermilab and, in particular, the 30-inch bubble chamber crew for their help with the data collection phase of this work.

REFERENCES

1. G. A. Smith, AIP Conference Proceedings No. 14, Particles and Fields - 1973 (APS/DPF Berkeley), ed. by H. H. Bingham, M. Davier and G. R. Lynch, p. 500; F. Svrcek and G. Zorn, Univ. of Md., Tech. Report No. 73-091 (1973); F. Ogino, "Proton-Proton Interactions at 200 and 300 GeV/c," Ph.D. thesis, Iowa State Univ. (1975).
2. L. Foa, Phyiscs Reports 22C (1975) 1.
3. J. Whitmore, Physics Reports 10C (1974) 273.
4. Z. Koba et al., Phys. Lett. 38B (1972) 25.
5. S. Barish et al., Phys. Rev. D9 (1974) 2689; A. Firestone et al., Phys. Rev. D10 (1974) 2080.
6. B. Alper et al., Nucl. Phys. B100 (1975) 237; P. Capiluppi et al., Nucl. Phys. B79 (1974) 189.
7. R. P. Feynman, Phys. Rev. Lett. 23 (1969) 1415; J. Benecke et al., Phys. Rev. 188 (1969) 2159; A. H. Mueller, Phys. Rev. D2 (1970) 2963.
8. V. A. Bumazshnov et al., Phys. Lett. 50B (1974) 283; V. V. Babintsev et al., "Inclusive and Semi-Inclusive Two Particle Correlations at 69 GeV/c," paper submitted to the XVII International Conference on High Energy Physics, London (1974); C. Bromberg et al., Nucl. Phys. B107 (1976) 82.
9. D. B. Smith et al., Phys. Rev. Lett. 23 (1969) 1064; D. B. Smith UCRL - 20632 (1971).
10. R. Schindler et al., Phys. Rev. Lett. 33 (1974) 862; J. Whitmore et al., Phys. Lett. 60B (1976) 211.

11. Z. M. Ma et al., Phys. Rev. Lett. 31 (1973) 1320.

12. T. Ferbel, Phys. Rev. Lett. 29 (1972) 448.

13. P. Carruthers and M. Duong-van, Phys. Rev. D8 (1973) 859.

14. R. J. Yaes, Phys. Rev. Letters 36 (1976) 821.

15. Z. Koba et al., Nucl. Phys. B40 (1972) 317.

16. P. Slattery, Phys. Rev. D7 (1973) 2073.

Table 1. Numbers of Events Used in This Analysis

n_-	200 GeV/c	300 GeV/c
1	3544	3861
2	3605	4402
3	1468	962
4	1027	711
5	592	508
6	328	318
7	147	185
8	60	78
9	15	50
10	2	13
11	3	3
12	-	5
sum	10791	11096

Table 2. n_- at Various Energies[a] having Equivalent Values of $z = n_-/\langle n_- \rangle$

Data Set	z	P_{inc}(GeV/c)				
		21	24	28.5	200	300
a	0.8			1		2-3
b	0.9	1			2-3	3
c	1.5			2		5
d	1.6		2		4-5	
e	1.8	2			5	6
f	2.3			3	6-7	7-8
g	2.4		3		7	8
h	2.6	3			7-8	8-9

[a] $\langle n_- \rangle$'s at 21, 24, 28.5, 200 and 300 GeV/c are 1.15, 1.24, 1.30, 2.84 and 3.25, respectively.

FIGURE CAPTIONS

Figure 1. (a) $d\sigma/dy_{lab}$ at 28.5,200 and 300 GeV/c; (b) $d\sigma/dp_T^2$ at 28.5, 200 and 300 GeV/c. Also shown is $d\sigma/dp_T^2$ for $y_{lab} < 1$.

Figure 2. $F_n(y_{lab}) = (d\sigma_n/dy_{lab})/\sigma_n$ versus n_- at 200 and 300 GeV/c. Lower energy data at equivalent $z = n_-/\langle n_-\rangle$ values are also plotted.

Figure 3. $G_n(p_T^2) = (d\sigma_n/dp_T^2)/\sigma_n$ versus n_-.

Figure 4. $F_n(y_{lab},s)$ at different z values. (a-h) refer to the data sets listed in Table 2.

Figure 5. $G_n(p_T^2,s)$ for $y_{lab} < 1$ for the same data sets as in Fig. 4.

Figure 6. $F_n(y_{lab},s)$ versus z for different y_{lab} regions.

Figure 7. (a) $F_n(y_{cm}=0)$, (b) $G_n(p_T^2=0)$, (c) the full width at half maximum (FWHM) of F_n and (d) $\langle p_T^2\rangle$, all plotted versus n_-.

Figure 8. $F_n(y_{cm}=0)$ versus $\ln^{-1}(E_a^2/m_p^2)$ for various values of n_-.

Figure 9. $\frac{d\sigma}{dy}$ at $y_{cm}=0$ versus $s^{-1/4}$. The solid curve is a calculation of Eqs. (8-10). The dotted curve for comparison is a similar calculation without the $0.05\ n_-^2$ term in eq. (8).

Figure 10. The gaussian width of the inclusive rapidity distribution. The solid curve is obtained from Eqs. (8-10). The dotted curve is the prediction of the hydrodynamic model.

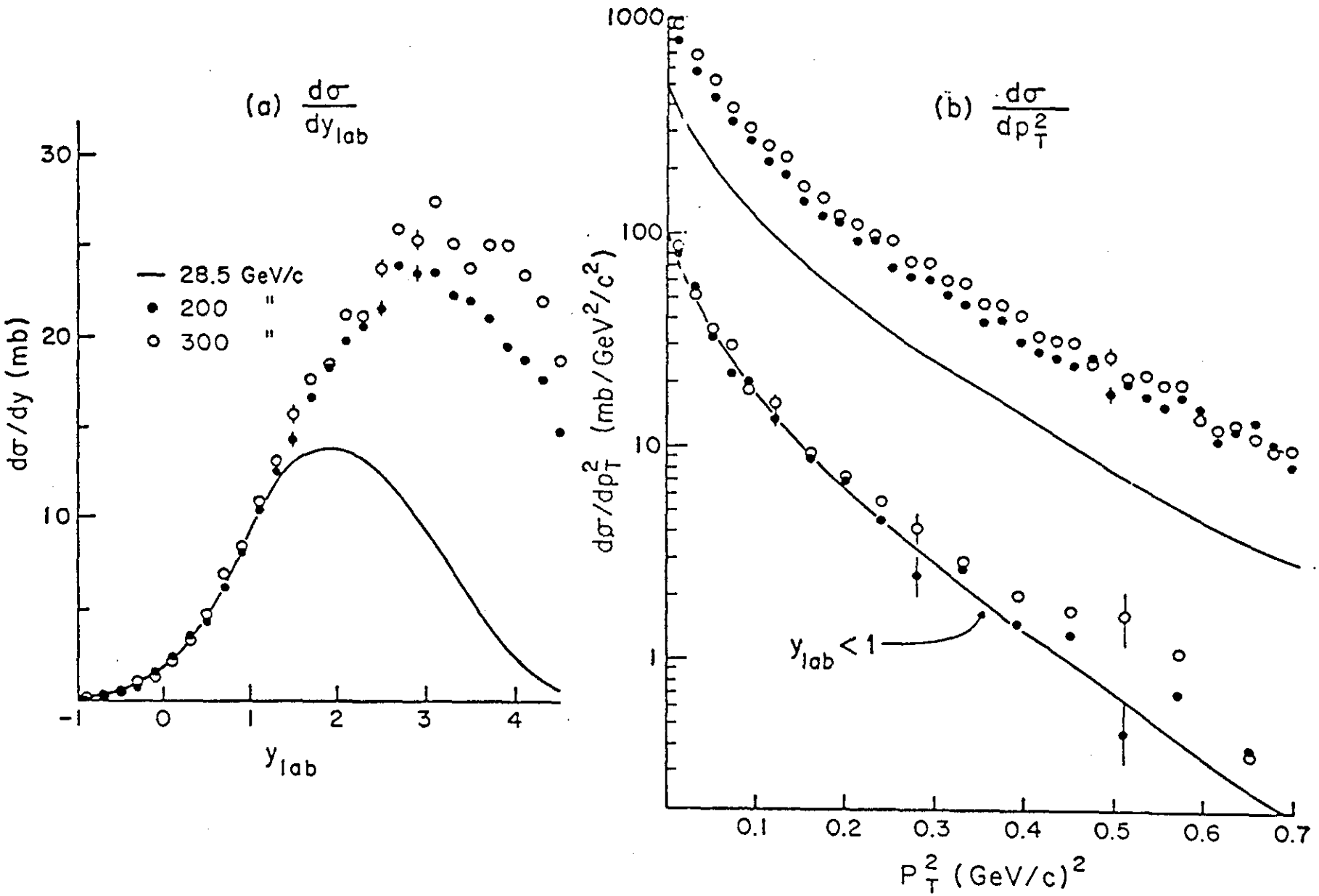
(a) $\frac{d\sigma}{dy_{lab}}$
28.5 GeV/c
200 "
300 "
$d\sigma/dy$ (mb)
y_{lab}
(b) $\frac{d\sigma}{dp_T^2}$
$d\sigma/dp_T^2$ (mb/GeV^2/c^2)
$y_{lab} < 1$
P_T^2 (GeV/c)^2

Figure 1

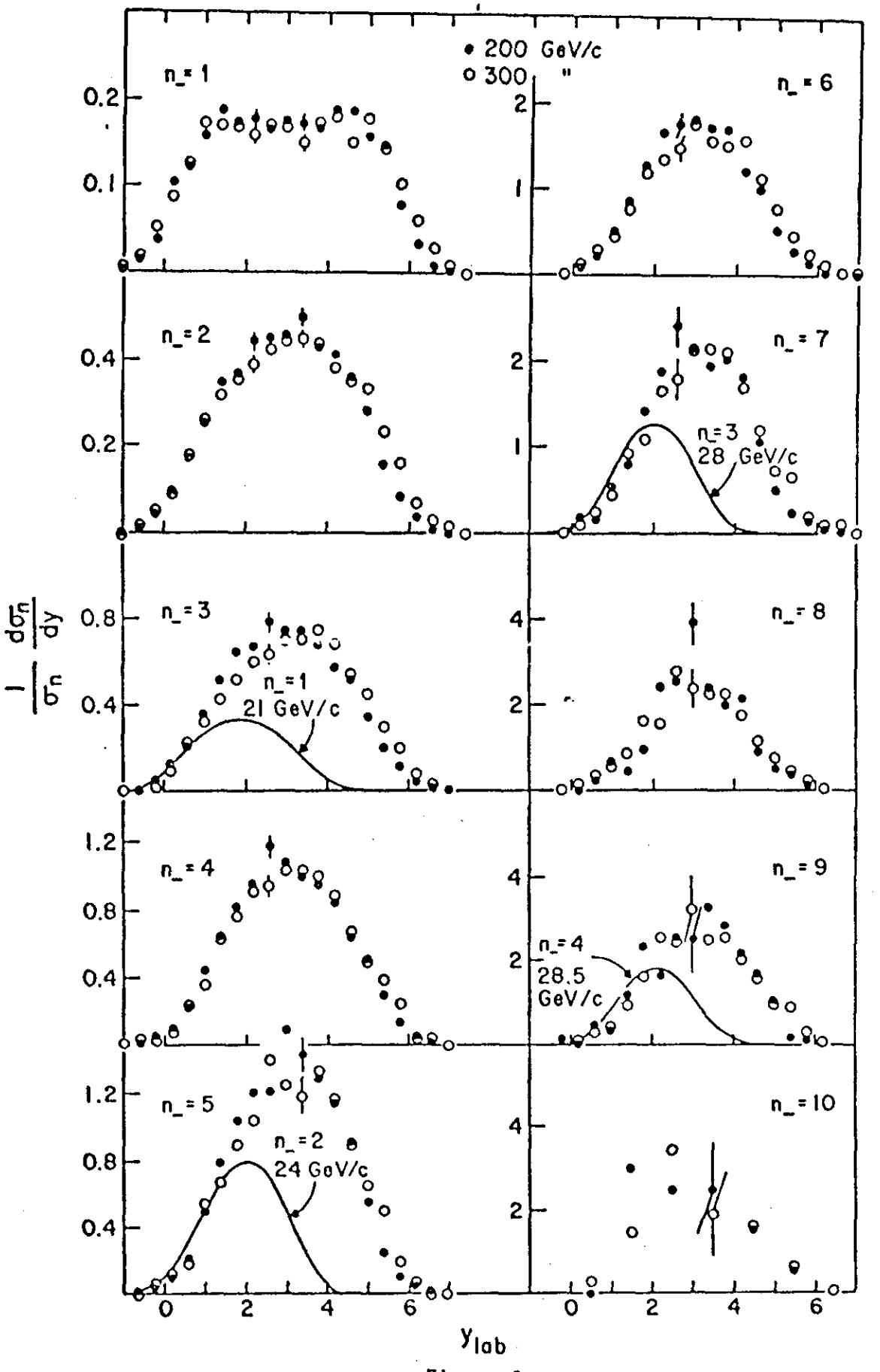
• 200 GeV/c
o 300 "
n_ = 1
n_ = 2
n_ = 3
n_ = 4
n_ = 5
n_ = 6
n_ = 7
n_ = 8
n_ = 9
n_ = 10
n_=1
21 GeV/c
n_=2
24 GeV/c
n_=3
28 GeV/c
n_=4
28.5
GeV/c
$\frac{1}{\sigma_n}\frac{d\sigma_n}{dy}$
y_{lab}

Figure 2

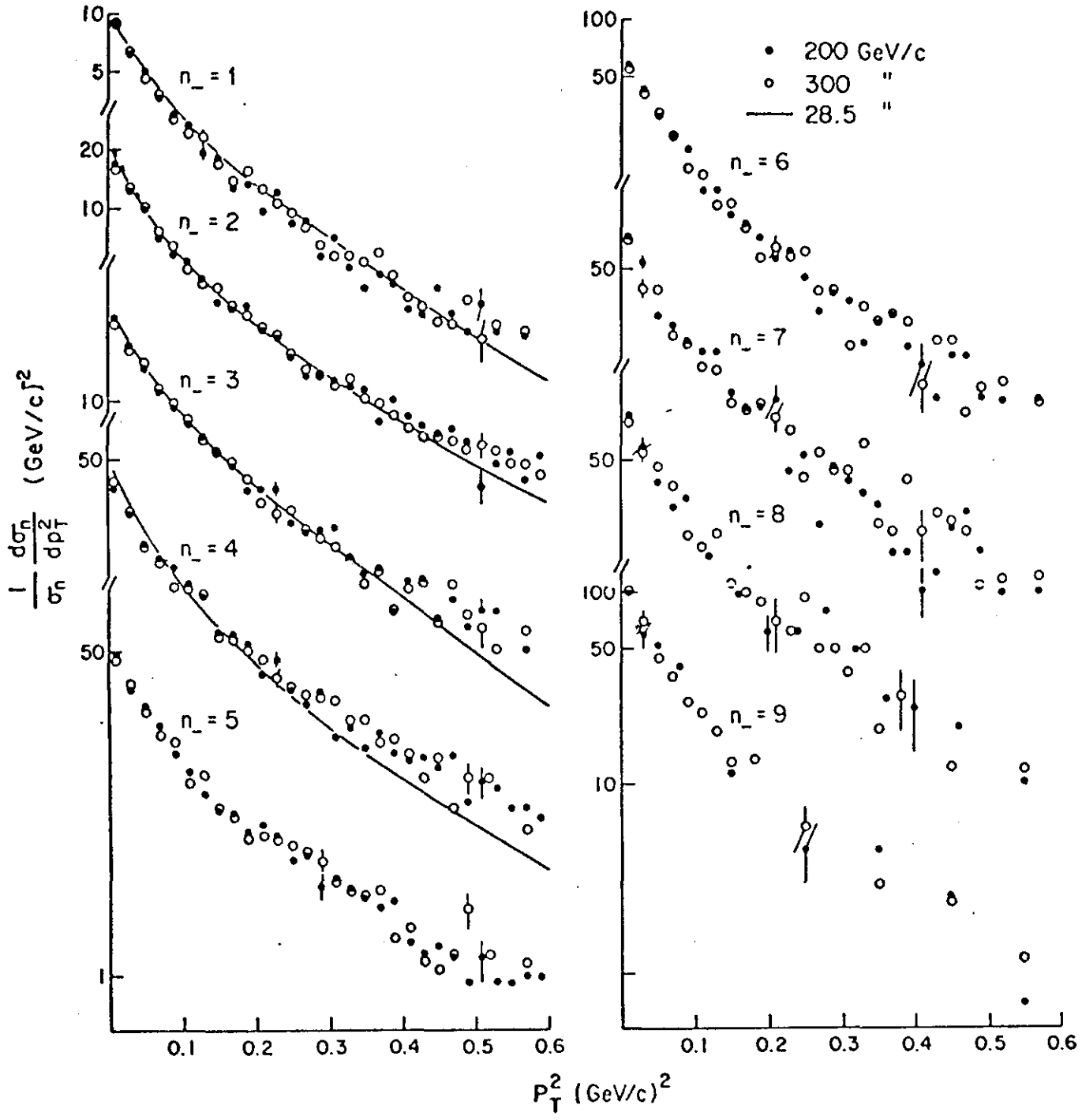
200 GeV/c
300 "
28.5 "
n_ = 1
n_ = 2
n_ = 3
n_ = 4
n_ = 5
n_ = 6
n_ = 7
n_ = 8
n_ = 9
$\frac{1}{\sigma_n}\frac{d\sigma_n}{dp_T^2}$ (GeV/c)^2
P_T^2 (GeV/c)^2

Figure 3

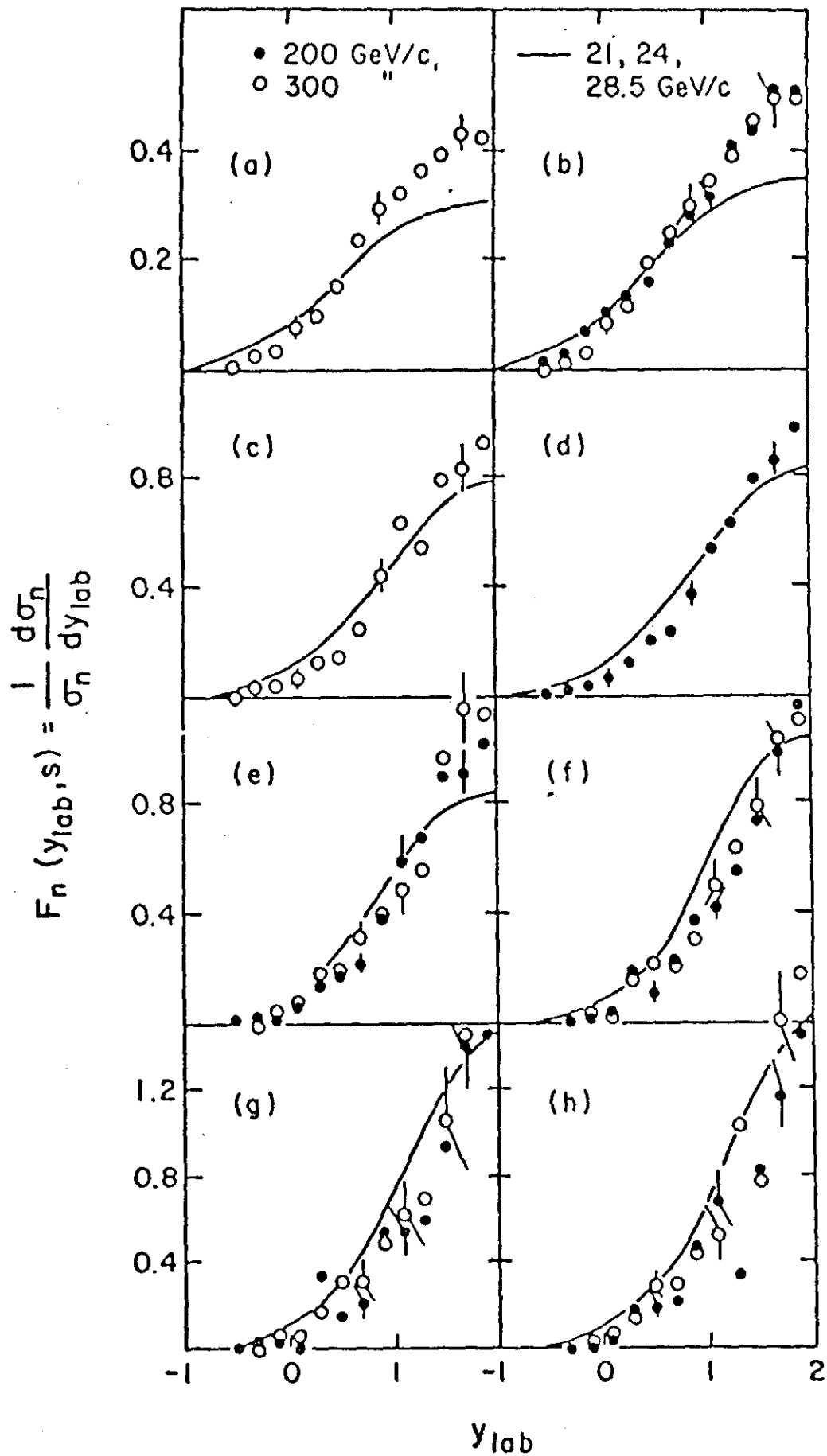
• 200 GeV/c,
○ 300 "
— 21, 24,
28.5 GeV/c
(a)
(b)
(c)
(d)
(e)
(f)
(g)
(h)
0.4
0.2
0.8
0.4
0.8
0.4
1.2
0.8
0.4
-1
0
1
-1
0
1
2
$F_n(y_{lab}, s) = \frac{1}{\sigma_n} \frac{d\sigma_n}{dy_{lab}}$
y_{lab}

Figure 4

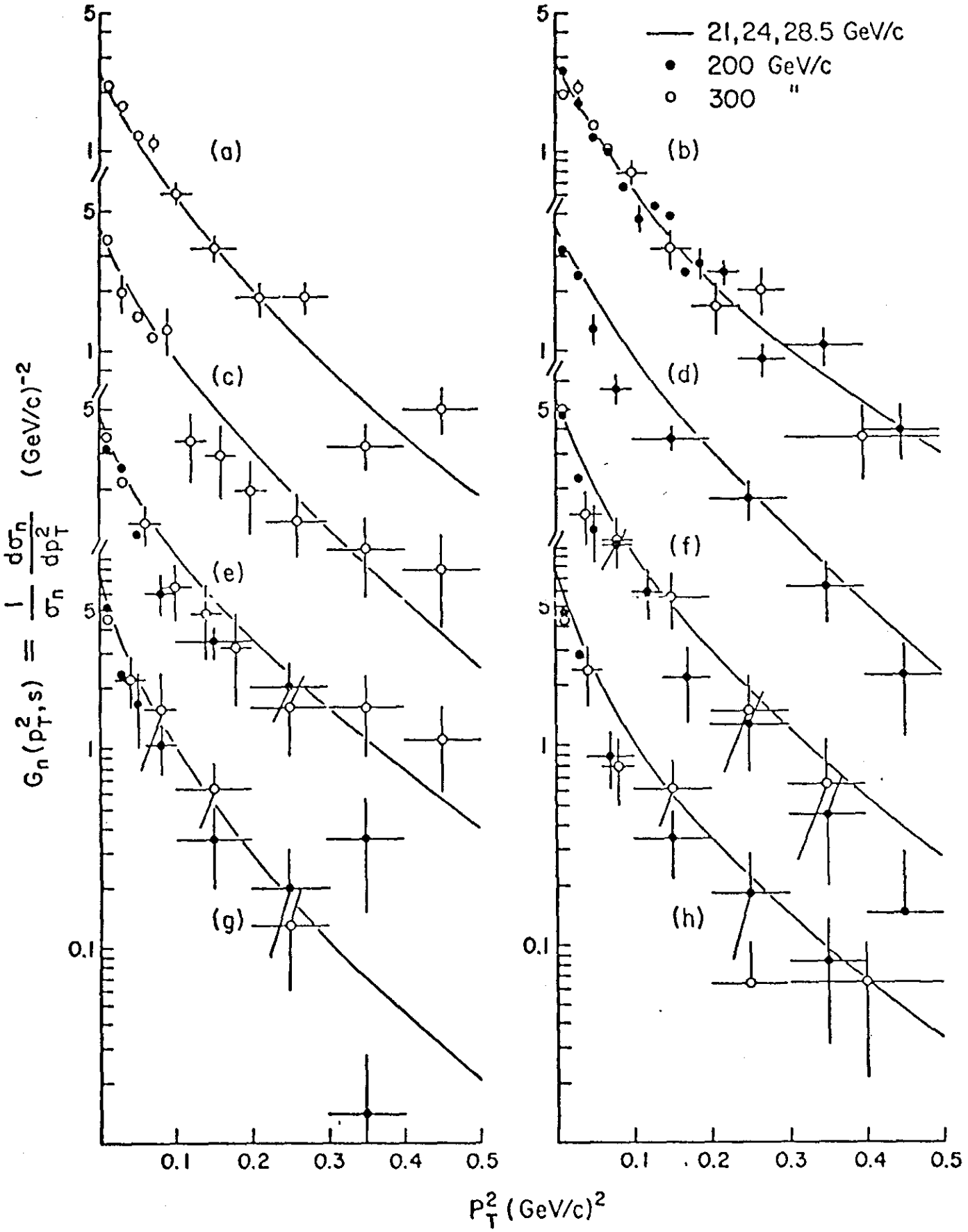
21,24,28.5 GeV/c
200 GeV/c
300 "
(a)
(b)
(c)
(d)
(e)
(f)
(g)
(h)
$G_n(p_T^2, s) = \frac{1}{\sigma_n} \frac{d\sigma_n}{dp_T^2}$ (GeV/c)$^{-2}$
P_T^2 (GeV/c)^2
5
1
0.1
0.1
0.2
0.3
0.4
0.5

Figure 5

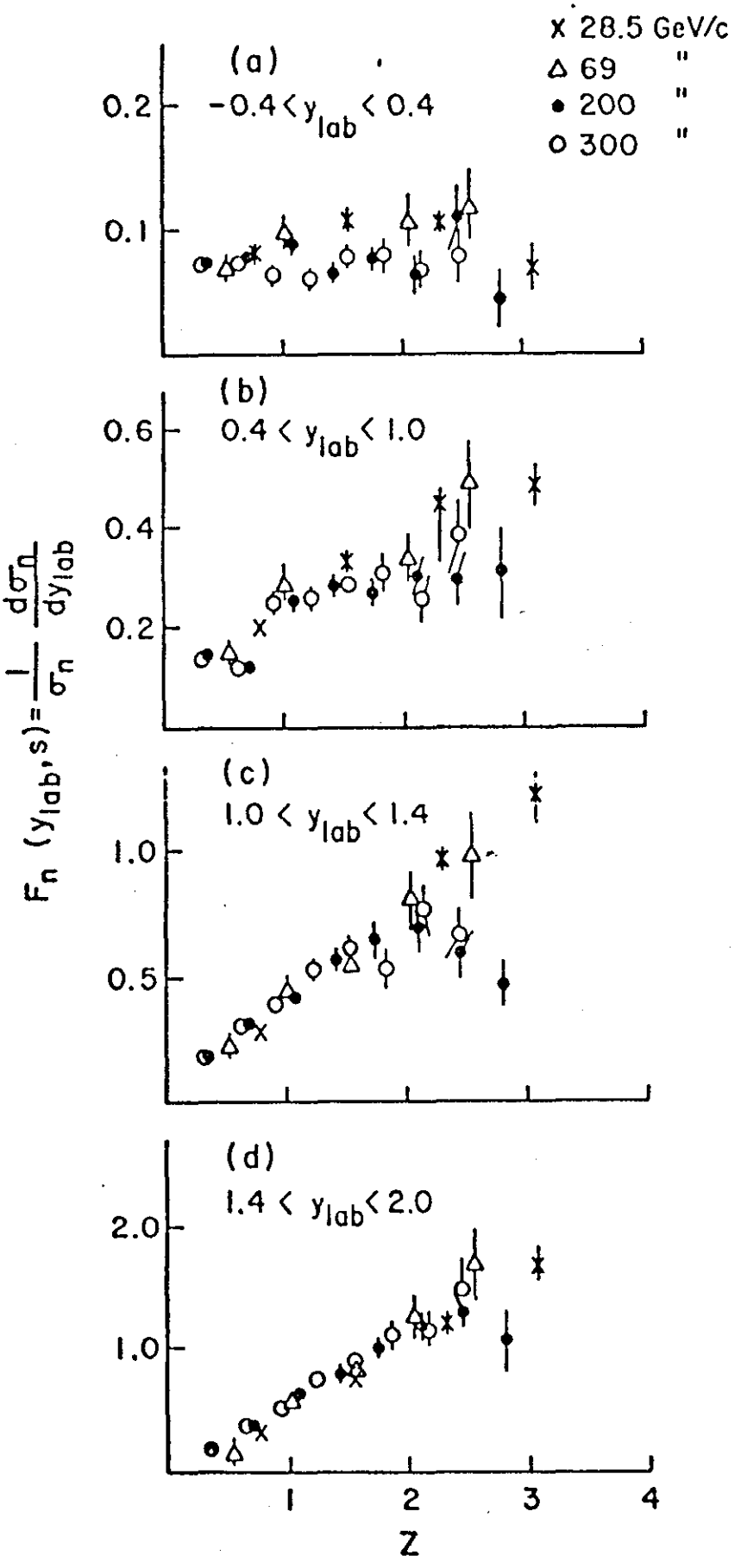
x 28.5 GeV/c
△ 69 "
● 200 "
○ 300 "
(a)
-0.4 < y_lab < 0.4
0.2
0.1
(b)
0.4 < y_lab < 1.0
0.6
0.4
0.2
(c)
1.0 < y_lab < 1.4
1.0
0.5
(d)
1.4 < y_lab < 2.0
2.0
1.0
F_n (y_lab, s) = 1/σ_n dσ_n/dy_lab
1
2
3
4
Z

Figure 6

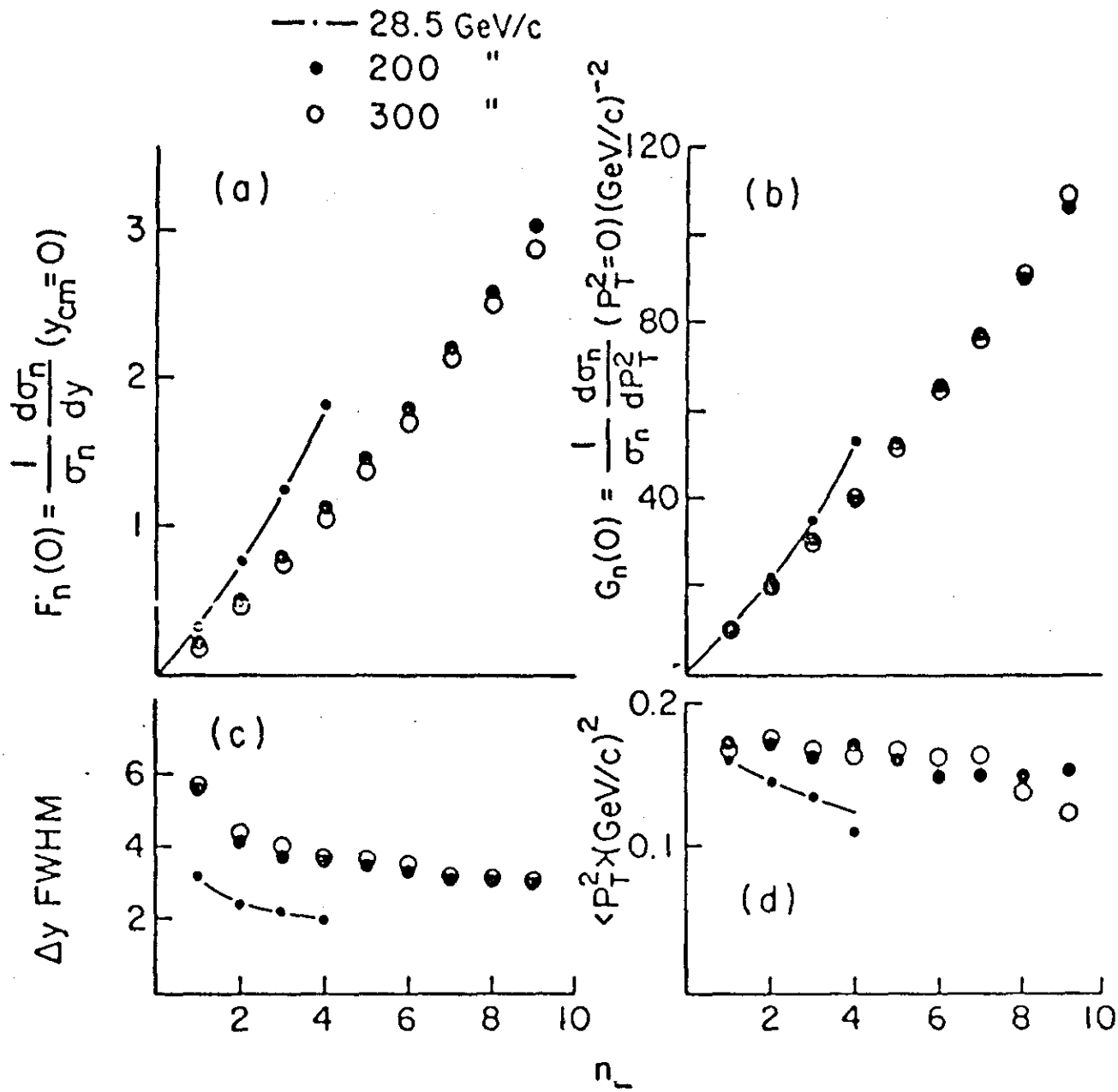
28.5 GeV/c
200 "
300 "
(a)
(b)
(c)
(d)
$F_n(0) = \frac{1}{\sigma_n}\frac{d\sigma_n}{dy}(y_{cm}=0)$
$G_n(0) = \frac{1}{\sigma_n}\frac{d\sigma_n}{dP_T^2}(P_T^2=0)(GeV/c)^{-2}$
Δy FWHM
$\langle P_T^2 \rangle (GeV/c)^2$
n_-

Figure 7

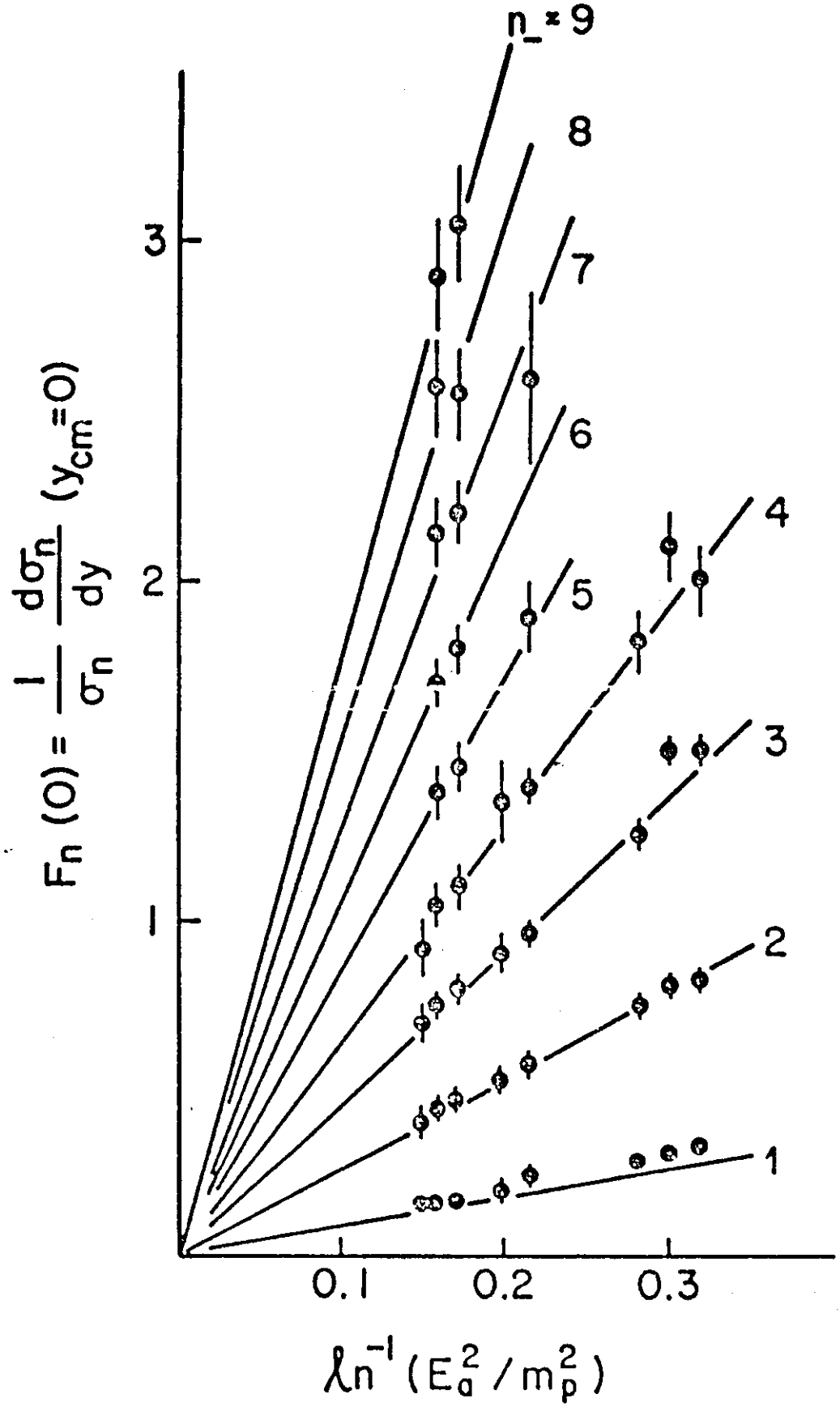
n_ = 9
8
7
6
5
4
3
2
1
3
2
1
0.1
0.2
0.3
$F_n(0) = \frac{1}{\sigma_n} \frac{d\sigma_n}{dy} (y_{cm}=0)$
$\ln^{-1}(E_a^2/m_p^2)$

Figure 8

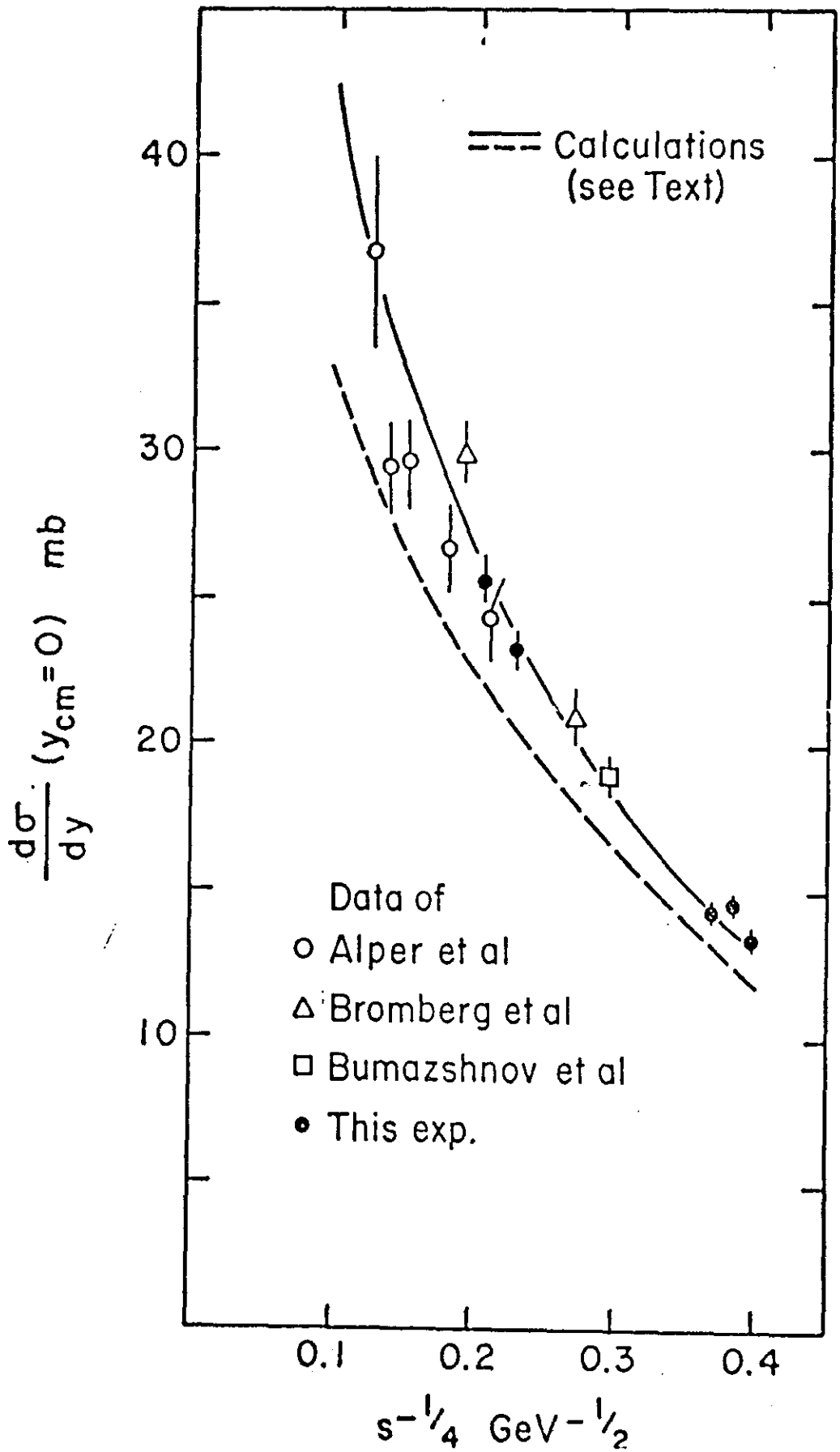
Calculations
(see Text)
Data of
Alper et al
Bromberg et al
Bumazshnov et al
This exp.
40
30
20
10
0.1
0.2
0.3
0.4
$\frac{d\sigma}{dy}(y_{cm}=0)$ mb
$s^{-1/4}$ GeV$^{-1/2}$

Figure 9

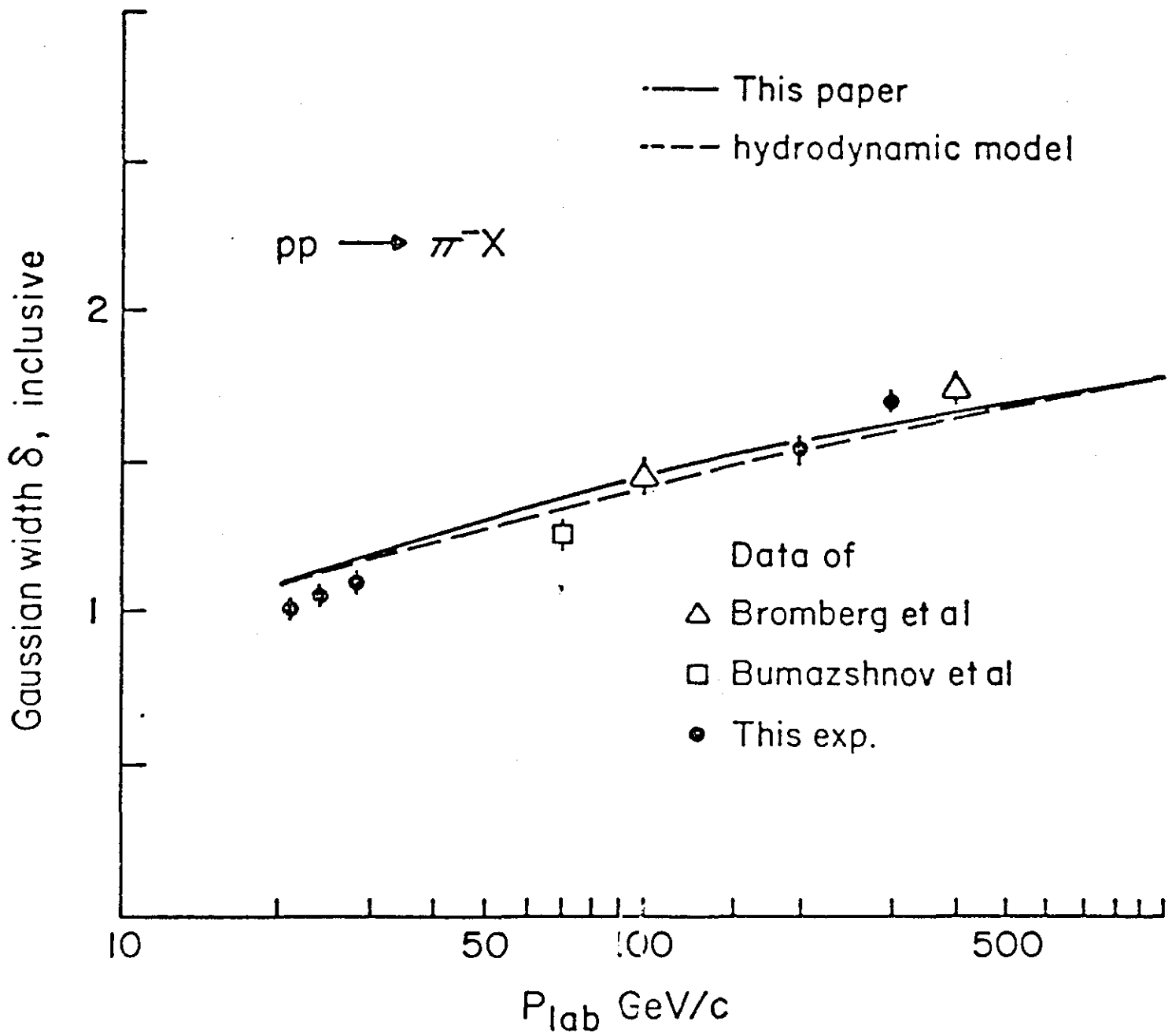
This paper
hydrodynamic model
pp → π⁻X
Gaussian width δ, inclusive
2
1
Data of
Bromberg et al
Bumazshnov et al
This exp.
10
50
100
500
P_lab GeV/c

Figure 10